High-resolution sub-ice-shelf seafloor records of 20th-century ungrounding and retreat of Pine Island Glacier, West Antarctica.

High-resolution sub-ice-shelf seafloor records of 20th-century ungrounding and retreat of Pine Island Glacier, West Antarctica

D. Davies[1], R.G. Bingham[1], A.G.C. Graham[2], M. Spagnolo[3,4], P. Dutrieux[5], D.G. Vaughan[6], A. Jenkins[6], F.O. Nitsche[5]

[1]School of GeoSciences, University of Edinburgh, Edinburgh, EH8 9XP, UK.
[2]College of Life and Environmental Sciences, University of Exeter, Exeter, EX4 4RJ, UK.
[3]School of Geosciences, University of Aberdeen, Aberdeen, AB24 3UF, UK
[4]Lamont-Doherty Earth Observatory of Columbia University, Palisades, New York, USA.
[5]Earth and Planetary Science Department, University of Berkeley, 94709, USA.
[6]British Antarctic Survey, Cambridge, CB3 0ET, UK.

Key Points:

- Ungrounding of Pine Island Glacier Ice Shelf from submarine ridge in 1940s left imprint of recent (de)glaciation on seafloor
- Sub-shelf bathymetric and sub-bottom profiling shows transition in bed properties across submarine ridge
- AUVs offer capability to image submerged deglaciated settings at resolution required for improved process understanding

Corresponding author: Damon Davies, `D.Davies@ed.ac.uk`

Abstract

Pine Island Glacier Ice-Shelf (PIGIS) has been thinning rapidly over recent decades, resulting in a progressive drawdown of the inland ice and an upstream migration of the grounding line. The resultant ice loss from Pine Island Glacier (PIG) and its neighboring ice streams presently contributes an estimated ∼10% to global sea-level rise, motivating efforts to constrain better the rate of future ice retreat. One route towards gaining a better understanding of the processes required to underpin physically-based projections is provided by examining assemblages of landforms and sediment exposed over recent decades by the ongoing ungrounding of PIG. Here we present high-resolution bathymetry and sub-bottom-profiler data acquired by autonomous underwater vehicle (AUV) surveys beneath PIGIS in 2009 and 2014 respectively. We identify landforms and sediments associated with grounded-ice flow, proglacial and subglacial sediment transport, overprinting of lightly-grounded ice-shelf keels and stepwise grounding-line retreat. The location of a submarine ridge (Jenkins Ridge) coincides with a transition from exposed crystalline bedrock to abundant sediment cover potentially linked to a thick sedimentary basin extending upstream of the modern grounding line. The capability of acquiring high-resolution data from AUV platforms enable observations of landforms and understanding of processes on a scale that is not possible in standard offshore geophysical surveys.

1 Introduction

The ice shelves that surround Antarctica's coast buttress ice flow from the continent's interior to the ocean [*Dupont and Alley*, 2005; *Fürst et al.*, 2016]. Over the last 25 years, however, many of the ice shelves along West Antarctica's Amundsen Sea margin have thinned extensively [*Pritchard et al.*, 2012; *Rignot et al.*, 2013; *Paolo et al.*, 2015], leading to progressive acceleration and surface lowering of ice inland [*Rignot et al.*, 2002; *Scott et al.*, 2009; *Wingham et al.*, 2009; *McMillan et al.*, 2014; *Mouginot et al.*, 2014; *Konrad et al.*, 2017], and an inland migration of the grounding line [*Park et al.*, 2013; *Rignot et al.*, 2014]. While the ice-shelf thinning has been attributed to sub-shelf melting [*Jacobs et al.*, 1996; *Pritchard et al.*, 2012; *Rignot et al.*, 2013], direct observations of the processes of sub-ice shelf melting and grounding-line retreat are few, because sub-shelf cavities are one of the Earth's least accessible environments [*Dowdeswell et al.*, 2008].

Only recently have autonomous underwater vehicles (AUVs) offered an opportunity to access sub-ice regions in Antarctica. Most sub-shelf AUV campaigns conducted to date have prioritized the measurement and characterization of sub-ice-shelf ocean-water properties and ice-shelf bases [*Nicholls et al.*, 2006; *Jenkins et al.*, 2010; *Jacobs et al.*, 2011; *Dutrieux et al.*, 2014a,b]. By contrast, comparatively little attention has been given to sounding or imaging seafloor bedforms and sediment properties beneath thinning ice shelves. Such settings, especially where ice has recently been grounded, provide opportunities to investigate âĂİgeomorphologically pristine,âĂİ recently-deglaciated terrains, and to relate these terrains to the processes that created them [e.g. *Domack et al.*, 2005; *Graham et al.*, 2013; *Smith et al.*, 2017].

In this paper, we present high-resolution bathymetry and sub-bottom-profiler data obtained by the Autosub3 AUV [*McPhail et al.*, 2009] beneath Pine Island Glacier Ice-Shelf (hereafter PIGIS), West Antarctica, during January 2009 and February-March 2014. Using these data we explore the nature of seafloor bedforms and sediment properties, and assess processes associated with retreat from a former pinning point during the mid-20th century. Our results reveal a suite of bedforms created by proglacial sedimentation, grounded ice flow and lightly-grounded ice flow, all reflecting the progressive ungrounding and retreat of Pine Island Glacier from beneath and just in front of the present ice shelf. We demonstrate the necessity to use meter-scale resolution imagery of recently-deglaciated terrains to understand processes of past decadal to centennial retreat.

2 Study area and geological context

PIGIS (Figure 1) impounds Pine Island Glacier (PIG), which together with Thwaites Glacier drain ~20% of the West Antarctic Ice Sheet (WAIS) into Pine Island Bay, the largest embayment of the Amundsen Sea. Since 1973 PIG's flux through PIGIS to the ocean has increased from 78 Gt yr^{-1} to ca. 133 Gt yr^{-1} [*Mouginot et al.*, 2014], an increase in ice transfer to the ocean of >40%. Between 1973 and 2010, the velocity of PIGIS increased by 1.7 km/yr or 75% and now flows at >4 km/yr [*Mouginot et al.*, 2014]. Contemporaneously, the ice has thinned progressively inland, with thinning now measurable at the ice divides [*Wingham et al.*, 2009; *Scott et al.*, 2009; *McMillan et al.*, 2014; *Konrad et al.*, 2017], and the grounding line has retreated 31 km between 1992 and 2011 [*Rignot et al.*, 2014]. Collectively, this is the most rapidly retreating region of ice on the planet, and is contributing an estimated ~5-10% of the currently observed global sea-level rise [*Rignot et al.*, 2008; *Turner et al.*, 2017].

PIG's current retreat is thought to have been triggered by ungrounding from a transverse submarine ridge, Jenkins Ridge (Fig.1), that spans the width of PIGIS ~30 km from the current grounding line [*Jenkins et al.*, 2010; *Smith et al.*, 2017]. Dating of sediments retrieved from the crest and seaward slope of Jenkins Ridge, via hot-water drilling through the ice shelf, suggests that ungrounding was initiated in the 1940s, and became complete by the 1970s [*Smith et al.*, 2017]. Satellite imagery also indicates that contact between the ice shelf and the highest point of Jenkins Ridge persisted in the early 1970s but became ungrounded in subsequent years [*Jenkins et al.*, 2010]. This ungrounding and retreat is associated with enhanced melting by incursion of warm Circumpolar Deep Water onto the continental shelf [*Jacobs et al.*, 2011; *Pritchard et al.*, 2012; *Hillenbrand et al.*, 2017]. Intermittent grounding of ice-shelf keels on localized bathymetric highs in the central region of PIGIS has also been detected within the last decade [*Joughin et al.*, 2016].

Regional geology is intrinsic to the properties of the seafloor beneath PIGIS. Upstream of the grounding line, relatively low crustal thickness in the PIG catchment observed in aero-gravity data facilitates ice streaming through the presence of thick sedimentary basins and elevated heat flux [*Jordan et al.*, 2009; *Muto et al.*, 2013, 2016]. The legacy of continental rifting associated with the formation of the West Antarctic Rift System [*Bingham et al.*, 2012] is a highly varied subglacial environment beneath PIG that exerts topographic controls on ice streaming [*Jordan et al.*, 2009]. Seward of PIGIS this regional topography contrasts between smooth sedimentary strata on the outer continental shelf and rough crystalline bedrock on the inner continental shelf in Pine Island Bay [*Jakobsson et al.*, 2011; *Nitsche et al.*, 2013]. Landforms on the outer continental shelf are dominated by mega-scale-glacial lineations (MSGL) associated with ice streaming over deforming sediments and grounding zone wedges (GZW) deposited during pauses in retreat of the Pine Island-Thwaites paleo-ice stream [*Anderson et al.*, 2002; *Lowe and Anderson*, 2002; *Graham et al.*, 2010; *Jakobsson et al.*, 2011]. The inner-continental shelf exhibits a more rugged seafloor charaterized by exposed crystalline bedrock streamlined by ice stream flow with deep (up to 1650 m) basins connected by meltwater channel networks [*Lowe and Anderson*, 2002; *Nitsche et al.*, 2013].

Because of the difficulty of accessing the sub-ice-shelf cavity, comparatively little is known about the detailed properties of the seafloor beneath PIGIS. Aero-geophysical surveys constrained by AUV and radar-soundings have provided broad insights into the sub-ice-shelf bathymetry and sediment distribution [*Studinger et al.*, 2010; *Muto et al.*, 2013, 2016]. These studies show that the Jenkins Ridge spans the entire ~45 km width of PIGIS and rises ~350-400 m above the seafloor. Landward of Jenkins Ridge lies a sedimentary basin up to ~800 m thick immediately upstream of the current grounding line, whereas sediments are absent or thin seaward of Jenkins Ridge [*Nitsche et al.*, 2013; *Muto et al.*, 2016].

AUV-mounted geophysical apparatus offers the ability to investigate the seafloor at sub-meter to meter-scale resolution [*Nicholls et al.*, 2006; *Wynn et al.*, 2014; *García et al.*, 2016]. Due to the challenging environment beneath Antarctic ice shelves and the operational and logistical limits of AUV operations, the spatial coverage of these data is limited. However, available data from missions beneath PIGIS thus far have provided insights into ocean properties in unprecedented detail [*Jenkins et al.*, 2010; *Jacobs et al.*, 2011; *Dutrieux et al.*, 2014a]. Sections of these data have received some geomorphological analysis [*Jenkins et al.*, 2010; *Graham et al.*, 2013], however a detailed study of seafloor geomorphology has not yet been conducted using the entirety of these datasets.

3 Data and Methods

3.1 Multibeam-swath bathymetry

High-resolution, sub-ice-shelf seafloor bathymetry covering a total distance of ~110 km (~3,850 km^2) of the seafloor was obtained from two AUV missions (M433 and M434) beneath PIGIS in January 2009 during Cruise NBP09-01 of the research icebreaker R/V Nathaniel B. Palmer (tracks marked in Figs.1a). Navigation is achieved by dead-reckoning through an Inertial Navigation System (INS), integrated and mechanically coupled with a downward looking Acoustic Doppler Current Profiler (ADCP). Navigational errors are typically between 0.2% and 0.1% of distance travelled [*McPhail*, 2009; *McPhail et al.*, 2009]. A Kongsberg EM-2000 multibeam echosounder was operated from the AUV at a nominal height of ~100 m above the seafloor which provides typical vertical root-mean square errors of <10 cm [*Dowdeswell et al.*, 2008]. Data were processed using MB-System, and a digital elevation model (DEM) was gridded with 2 m cell sizes using a weighted near-neighbor algorithm [*Graham et al.*, 2013; *Dutrieux et al.*, 2014b].

Figure 1. Map and locations of Autosub3 sub-ice shelf missions beneath Pine Island Glacier Ice-Shelf (PIGIS). a Sub-ice shelf bathymetry derived from gravity inversion (see supplementary material in *Dutrieux et al.* [2014a] for methodology) showing the location of Jenkins Ridge (JR) and Autosub3 mission tracks. Black line shows the ice-shelf front position in 2009. Boxes show areas covered by figures referred to later in text. Grounding line locations are from the MEaSUREs dataset [*Rignot et al.*, 2011]. **b**, Cross-section of ice and seafloor geometry extracted from profile y-y' (dashed black line) showing geomorphic zones 1-4 (ice draft and bathymetry from *Dutrieux et al.* [2014a]; see their supplementary material for methodology). Data for each zone are shown in Figs 2-4.

3.2 Sub-bottom profiling

Sediment properties were investigated using an Edgetech 2200M sub-bottom profiler mounted on Autosub3. Data were obtained from AUV deployments during the iSTAR research cruise JR294/295 from the RRS James Clark Ross in February and March 2014. The system emits a chirp signal at 2-16 kHz providing shallow penetration images of the seafloor with a resolution of 6-10 cm. Two missions (M447 and M448) covered ~150 km of the seafloor from ~20 km seaward of the 2009 ice front across the seaward slope, crest and backslope of Jenkins Ridge and into the ice-shelf cavity (Fig. 1a). A bandpass Butterworth filter with lower and upper cut-offs of 1000 and 3500 kHz respectively was applied to the data to remove high-frequency noise. A vertical correction was applied to account for the AUV's flying height. Water depths and sediment thickness were calculated by converting the two-way travel time to meters using acoustic velocities of 1459 m s^{-1} for water and 1500 m s^{-1} for soft unconsolidated sediment respectively. We provide an error margin of ±3% for estimates of sediment thickness as recommended by *LysÃě et al.* [2010].

Bathymetric data were not recorded concurrently with the sub-bottom profiler in 2014 due to problems encountered with the EM-2000 multibeam echosounder, and therefore we are unable directly to compare contemporaneous bathymetric and sub-bottom-profiler data. However, survey tracks M447 and M448 closely follow parallel to, and intersect, multibeam survey tracks M433 and M434 (Fig.1a).

3.3 Mapping and metrics

Geomorphological features were mapped from bathymetric DEMs in ArcGIS v.10.1. Multiple-illumination azimuths and vertical exaggerations were applied to aid visualization following the methods of *Smith and Clark* [2005]. To further aid mapping, subtle geomorphological features were accentuated using a surface-detrending algorithm that fitted a polynomial to the original DEM using a 30 m kernel window to produce a smoothed surface, which was then subtracted from the original DEM [*Hurst et al.*, 2012]. Three-dimensional surfaces were produced and visualized in Schlumberger Petrel™seismic interpretation software.

Linear bedforms were mapped by drawing lines across their crests while azimuths (0-360Âř from grid North) were extracted using GIS tools. Spacing and amplitude of linear bedforms were calculated by averaging multiple measurements extracted from cross-sectional topographic profiles transverse to bedform crestlines following the method of *Spagnolo et al.* [2014].

4 Results and Analysis

In this section we describe the seafloor bedforms and sediment properties imaged below PIGIS, respectively, in 2009 and 2014 using the techniques described above. Figure 2 provides an overview of bathymetric data showing relief-shaded DEMs alongside interpretations of landforms. We structure the findings by location relative to Jenkins Ridge, as demarcated on Figure 1b: progressively approaching the grounding line the zones can broadly be described as (1) the outer sub-ice-shelf seafloor, (2) the PIG-distal flank of Jenkins Ridge, (3) Jenkins Ridge crest, and (4) the PIGIS submarine cavity (Fig.1b). In the following sections we present seafloor bathymetry (Fig. 3) and sub-bottom profiler data (Fig. 4) in turn for each zone with the exception of Zone 4 where only sub-bottom profiler data were acquired.

Figure 2. Sub-ice-shelf multibeam-bathymetry data and geomorphological interpretation. a, Map of regional bathymetry and location of multibeam surveys M433 and M434. Red triangles show the locations of sediment cores described in [*Smith et al.*, 2017]. Black line shows the ice-shelf front position in 2009. **b-f**, Multi-directional relief-shaded multibeam topography plotted alongside corresponding geomorphological interpretations. Data width have been exaggerated by a factor of two for clarity. Black lines superimposed over debris flows delimit individual debris flow lobes. Black boxes show the location of three-dimensional surface imagery shown in Figure 3.

4.1 Zone 1:Outer sub-ice-shelf seafloor

4.1.1 Seafloor bathymetry

The regional bathymetry of Zone 1 exhibits rugged topography, likely dominated by outcrops of crystalline bedrock that rise in excess of 40 m above intervening smooth, flat-bottomed basins (Figs. 2b, c). The surfaces of outcrops in profile M433 host parallel lineations 2-10 m in amplitude and up to 1.5 km in length orientated along the trough axis (Fig.3b). The morphology of these features is consistent with streamlined-bedrock landforms described in offshore-bathymetry datasets in Pine Island Bay and on the inner continental-shelf region of the western Amundsen Sea Embayment [*Lowe and Anderson*, 2002; *Graham et al.*, 2009; *Nitsche et al.*, 2013].

Further south, and traversing an extensive basin, data from profile M434 exhibit lineations and outcrops truncated abruptly by steep-sided channels >200 m wide with curvilinear cross-sectional profiles (Figs. 2c; 3c,d). A series of irregular depressions up to 3 m deep and 150 m wide punctuates the crest of a lineation in this region (Fig. 3f). 6 km downstream from the location of these surface depressions is a chain of flat-topped mounds up to 10 m in height, 300 to 1000 m in width, and up to 2 km in length (Fig. 3d). The mounds' long axes generally trend parallel to inferred paleo-ice stream flow.

4.1.2 Sub-bottom profiler

The topography of the seafloor in Zone 1 imaged from the sub-bottom profiler further demonstrates the typical ruggedness of the former ice bed in this region as suggested by the bathymetric surveys (Fig. 4b). Regions of elevated seafloor are characterized by a high-amplitude, continuous acoustic reflector, between which some acoustically-stratified topographic depressions are interspersed (Fig. 4c). The stratification within each depression is characterized by a series of laterally continuous, parallel reflectors conforming to the underlying seafloor topography. The full sequence of stratified reflectors has a maximum thickness of 7.5 ± 0.2 m (Fig. 4c inset).

4.2 Zone 2:PIG-distal flank of Jenkins Ridge

4.2.1 Seafloor bathymetry

The transition between Zone 1 and Zone 2 is marked by an abrupt change from rugged to relatively smooth seafloor topography (Fig. 2d,e) reflecting an apparent shift to a sediment-dominated regime. Bedforms in Zone 2 broadly display amplitudes an order of magnitude lower than in Zone 1 and, on the whole, show little to no streamlining. Towards the base of Jenkins Ridge flank, on M433, a network of channels and ridges with a dendritic pattern cuts across the slope (Fig. 2d; zoom in Fig. 3e); individually they vary in size but typically have depths and amplitudes <2 m, and they cover a distance of at least 2800 m (~980 km^2) of the lower slope of Jenkins Ridge. Further upslope, irregular, undulating surfaces superimposed by lobate ridges (convex downslope) are more common (Fig. 2d; zoom in Fig. 3f).

Further south on the lower Jenkins Ridge flank (profile M434; Fig. 2h) is imaged a series of spherical mounds protruding 1-3 m from the seafloor and with a maximum diameter of ~20 m (profile left of panel 3h). Each mound is fringed by crescent-shaped ridges 1-1.5 m in amplitude. A pair of subtle, parallel, linear scours also occurs in close proximity to these boulders (Fig. 3h). They have a mean spacing of 49 m, amplitudes of <1 m, and lengths up to 650 m, and occur at depths of 950-970 m. The scours trend east-west as opposed to the more typical southeast-northwest direction of streamlined-bedform features observed seaward in Zone 1 (rose diagram right of panel h).

Near to the top of Jenkins Ridge's seaward flank, where the headroom between the former ice-shelf base and sea floor narrows, a set of seafloor lineations is also observed, exhibiting orientations in line with modern ice flow vectors (Fig. 2d; zoom in Fig. 3g). The lineations have spacings of 19-36 m (mean 26 m), amplitudes of <1 m, and lengths up to 600 m. They are located 2.5 km west of sediment cores that date ungrounding of the ice shelf from Jenkins Ridge to 1970 ±4 years (Fig. 2a) [*Smith et al.*, 2017].

4.2.2 Sub-bottom profiler

The transition between Zone 1 and 2 is marked by a change in the character of the seafloor acoustics from a rugged interface with some sub-surface structure to an acoustically-transparent unit with a diffuse seabed reflector (Fig. 4d). The seabed within this zone is predominantly smooth with some small-scale lobes or mounds up to ~3 m in amplitude (Fig.4e).

4.3 Zone 3: Jenkins Ridge crest

4.3.1 Seafloor bathymetry

Only profile M434 provides data from Zone 3: the AUV imaged data along an ~8 km long strip broadly along-paleo-ice-flow, and a ~13 km long strip along the southern half of Jenkins Ridge crest trending broadly orthogonal to current ice-shelf flow (Fig. 2f). Along the entire Jenkins Ridge crest the predominant geomorphological feature comprises streamlined lineations oriented parallel to inferred paleo-ice-flow (Figs. 3i, j). A change in the metrics of these lineations is clearly evident ~6 km along the profile (north to south), coinciding with a sharp rise in seafloor elevation from a mean of -730 m to -708 m (Fig. 5a). In the northern section, closer to the central flow-axis of PIGIS, the lineations have a mean spacing of 287 m and mean amplitude of 7.3 m; in the southern section they have a mean spacing of 46 m and a mean amplitude of 1.4 m (Fig. 5b,c). Furthermore, along the southern section of Jenkins Ridge crest, not all the lineations are parallel to one another, and occasionally they appear to cross-cut or converge (Magnified panel in Fig. 3j).

The surface characterized by lineations that we have just described is overprinted by finer-scale features. These include sub-meter-amplitude curvilinear sediment ridges that are convex in the direction of paleo-ice flow and have spacing of 26-90 m (mean 43 m) (left-hand zooms in Fig. 3i). The curvilinear ridges initiate at the bases of lineation-troughs and terminate at the apexes of their crests. Curvilinear ridges of this scale and character have not, to our knowledge, been observed elsewhere in glacial settings. Erosional scours with troughs up to 7 m deep also occur at the crests of some lineations and terminate in small-scale asymmetric berms (right-hand zooms in Fig. 3i).

4.3.2 Sub-bottom profiler

A 20 km section of profiler data from mission M448 trending southwest to northeast crossed the crest of Jenkins Ridge (Fig. 4f). The ridge surface is characterized by an undulating high-amplitude seafloor reflector (Fig. 4f). Smaller scale ridges with a mean amplitude of 4 m are superimposed on this surface and have a similar cross-sectional profile to the seabed of survey M434 in Zone 3 (Fig. 5a).

Figure 3. Three-dimensional surfaces of multibeam seafloor bathymetry.**a**, inset map showing the locations of panels b-j. Multibeam surface imagery of seafloor topography and extracted topographic profiles in Zone 1 (b-d), Zone 2 (e-h) and Zone 3 (i and j). Location of panel h is shown in the inset map and Figure 2e. Rose diagram next to panel h shows the azimuth of lineations sampled from Zones 1-3 compared to linear scours in panel h.

4.4 Zone 4:PIGIS submarine cavity

4.4.1 Sub-bottom profiler

The morphology and acoustic character of the reverse slope of Jenkins Ridge in the ice-shelf cavity are similar to those of the seaward slope in Zone 2, although there is no evidence for mass-movement deposits on this side of the ridge. At the easternmost limit of the survey, approximately 15 km seaward of the grounding line, a series of ridges with asymmetric cross-sectional profiles, ranging between ~7 and 28 m in amplitude, is imaged (Fig. 4i). A series of shorter wavelength, lower amplitude, regularly spaced ridges caps the crest of the largest of these asymmetric ridges (Fig. 4i, j).

Figure 4. Acoustic sub-bottom profiler data. a, Map of regional bathymetry and location of sub-bottom profiler surveys beneath Pine Island Glacier Ice-Shelf. Black boxes denote sections of data shown in the main figure. **b**, Rugged seafloor topography and acoustically stratified basins (black arrows) in Zone 1. **c**, close-up of an acoustically stratified basin showing up to 7.5 m of stratified sediments. Sediment thickness was calculated using an acoustic velocity of 1500 m s^{-1} for sediments. **d**, acoustically transparent seafloor reflector of the seaward flank of Jenkins Ridge. **e**, Close-up showing debris flow lobes (black arrows). **f**, profile across Jenkins Ridge showing a strong surface reflector and undulating seafloor. **g**, Close-up showing mega-scale glacial lineations (black arrows). **h**, acoustically transparent seafloor reflector on the inland slope of Jenkins Ridge. **i**, Close-up view of asymmetric ridges. **j**, Close-up of corrugation ridges overprinting the crest of asymmetric ridges.

5 Discussion

5.1 Interpretation of bedforms and sediment properties

From the combined evidence presented above from beneath PIGIS we identify three distinct components of the sub-ice-shelf landsystem that we associate with 1) grounded ice

Figure 5. Landform metrics of Jenkins Ridge crest. a, Topographic profile of seafloor elevation across the crest of Jenkins Ridge (Zone 3). Blue line shows detrended seafloor topography. Grey shaded area shows the region defined as Z3 North based on a change in landform metrics. **b,c,** Box and whisker plots showing the median, lower and upper quartile and standard deviation of lineation spacing and amplitude of 52 lineations sampled across the ridge crest. A summary of statistics is presented in Table 1 in text.

flow, 2) lightly-grounded ice flow and 3) postglacial deposition. Synthesized maps of bedform interpretations presented alongside the multibeam data in Figure 2 provide a useful reference for this discussion.

5.1.1 Grounded-ice bedforms

We interpret a suite of bedforms in Zones 1, 3 and 4 as resulting from subglacial erosion, sediment deposition and meltwater flow beneath grounded ice. Due to their curvilinear cross-sectional profiles, steep-sided channels in Zone 1 (Fig. 3c,d) are interpreted as relict subglacial meltwater channels eroded into the substrate when more advanced ice was grounded here during one or more earlier glacial phases [c.f., *Wellner et al.*, 2006; *Nitsche et al.*, 2013]. The irregular surface depressions in Figure 3c bear resemblance to hill-hole pairs observed in bathymetric data in the Norwegian Channel where they are thought to represent the imprint of sediment slabs that froze onto the glacier sole and were removed/displaced [*Ottesen et al.*, 2016]. However, if the surface depressions in Figure 3c are similarly interpreted as hill-hole pairs, their estimated volumes are an order of magnitude smaller than those observed in the Norwegian Channel. Flat-topped mounds (Fig. 3d), which we interpret as glacitectonic rafts [*Andreassen et al.*, 2004; *Rüther et al.*, 2013; *Rüther et al.*, 2016], are most likely related to a displacing process similar to that which caused the formation of the hill-hole pairs. Because freeze-on is predominantly associated with thin ice (<1 km) close to the glacier margin [*Moran et al.*, 1980; *Alley et al.*, 1997] it is likely that these features were formed when the grounding line was located nearby, and before it became pinned to the crest of Jenkins Ridge.

Ubiquitous lineations on the crest of Jenkins Ridge (Zone 3; Figs. 2f and 3i, j [multibeam imaging]; and 4f [sub-bottom-profiling]) are also the result of formerly-grounded ice flow. To the north, their amplitude and spacing are consistent with dimensions of mega-scale glacial lineations (MSGL) [*Clark*, 1993; *Spagnolo et al.*, 2014] (Table 1). Although

Table 1. Summary statistics of lineations in Zone 3 compared to previously published metrics of mega-scale glacial lineations and flutes

	Z3 North lineations (this study) n=16	Z3 South lineations (this study) n=36	MSGL [Spagnolo et al., 2014] n=4043	Flutes [Ely et al., 2016] n=88
SPACING (m)				
Minimum	129.8	13.6	-	-
Maximum	569.7	159.8	-	-
Mean	287.2	46.3	458	-
Median	265.0	32.8	330	-
Std. Deviation	121.7	34.8	-	-
AMPLITUDE (m)				
Minimum	3.4	0.2	-	0.02
Maximum	15.2	5.0	-	0.3
Mean	7.3	1.4	4	0.01
Median	6.7	1.0	3	-
Std. Deviation	3.0	1.2	-	0.07

we are unable to determine the lengths of these individual bedforms from our dataset, a section of bathymetry data along-flow described by *Graham et al.* [2013] captured two lineations with lengths of at least 1800 m. This implies elongation lengths of at least 9:1 and probably greater, a characteristic of elongated streamlined bedforms described beneath paleo- and modern ice streams [*King et al.*, 2009; *Spagnolo et al.*, 2014]. Ridges parallel to paleo-ice flow imaged in sub-bottom-profiler data over the crest of Jenkins Ridge (Fig. 4g) have comparable amplitudes to ridges observed in the bathymetric data. Although it is not possible to determine their three-dimensional morphology, it is likely they are a continuation of MSGL identified in the northern section of Zone 3 (Fig 3i).To the south, linear bedforms on Jenkins Ridge have a much shorter wavelength and reduced amplitude intermediate between MSGL and flutes (Table 1., Fig. 5). We consider this change in metrics to be related to a change in till strength or thickness towards the margin of the ice-stream trough.

Four asymmetric ridges oriented across former flow in Zone 4 with amplitudes of 5-20m (Fig. 4h,i) are morphologically similar to small retreat moraines and back-stepping grounding-zone wedges (GZWs) observed on the seafloor in the Ross Sea [*Halberstadt et al.*, 2016; *Simkins et al.*, 2016]. Their location close to the modern grounding line suggests that these features were formed in the last 40-70 years through sediment deposition during a series of pauses in grounding-line retreat. Multibeam coverage is needed to verify these observations but, if our interpretation is correct, this indicates the rate of grounding-line retreat has not been constant since ungrounding from Jenkins Ridge. Sub-bottom reflectors dipping at angles greater than the seabed surface slope are also evident on the landward slope of the largest asymmetric ridge, suggesting a sediment history is preserved in the cavity close to the grounding line (Fig. 4i).

5.1.2 Lightly-grounded-ice bedforms

On Jenkins Ridge crest, we interpret the ridges and scours that overprint MSGL (zooms in Fig. 3i) as forming by sediment squeezing of lightly-grounded ice-shelf keels, modulated by tidal motion as suggested by *Graham et al.* [2013]. Some corrugation ridges with amplitudes between 0.5-2 m have been imaged ~360 km northwest of the grounding line in Pine Island Trough [*Jakobsson et al.*, 2011] and in the Ross Sea [*Shipp et al.*, 1999; *Anderson et al.*, 2014; *Halberstadt et al.*, 2016]; the potential corrugation ridges on Jenkins Ridge have amplitudes <1 m with spacing and amplitude varying along the ridge crest (zooms in Fig. 3j). This may be related to variable ice-keel morphology as identified by multibeam observations of basal terraces beneath PIGIS [*Dutrieux et al.*, 2014b]. However, substantial sub-ice shelf melting since ungrounding from Jenkins Ridge will have altered the basal morphology of the ice shelf compared with the formerly grounded ice keels. This prohibits any direct comparison between corrugation and sub-ice shelf morphology.

The scours (right-hand zooms in 3i) are comparable to iceberg ploughmarks observed in water depths in excess of 700 m on the continental shelf and interpreted to have been caused by incision of iceberg keels where they contact the sea floor [*Dowdeswell and Bamber*, 2007; *Gales et al.*, 2016]. For iceberg keels to be the mechanism of formation here would require the crest of Jenkins Ridge to have been subject to grounding of free floating icebergs at some point since ungrounding of PIGIS in the 1970s. However, remote sensing imagery shows PIGIS has remained intact throughout this period. We therefore favor forward ploughing of ice-shelf keels as the most likely mechanism for their formation. The alignment of scours parallel to the direction of present ice shelf flow also supports this. Terminal berms associated with these scours (zoom in Fig. 3i) are likely to have been created when ice-shelf keels that were last in contact with the crest of Jenkins Ridge became ungrounded.

5.1.3 Postglacial processes

Postglacial deposition is evident in the most distal regions from the current grounding line. In Zone 1, contrasting stratified reflectors in sub-bottom-profiler data are interpreted as alternations between coarse-grained ice-rafted/ice-shelf basal debris and fine-grained hemipelagic sediments from meltwater plumes [c.f. *Damuth*, 1978; *Batchelor et al.*, 2011; *Rebesco et al.*, 2011; *Hogan et al.*, 2012].

Bedforms on the seaward flank of Jenkins Ridge in Zone 2 are dominated by postglacial slope processes. Dendritic channels and ridges are morphologically characteristic of sediment-gravity flows commonly observed in trough-mouth fan (TMF) and continental-shelf-break settings [*Dowdeswell et al.*, 1998; *Vorren and Werner*, 1998; *Dowdeswell et al.*, 2004; *Amblas et al.*, 2006] and on the distal flanks of submarine terminal moraine ridges in fjord settings [*Ottesen and Dowdeswell*, 2006; *Dowdeswell et al.*, 2016]. We interpret the lobate, curvilinear ridges on the seaward flank of Jenkins Ridge (zoom in Fig. 3f) as submarine debris flows, also observed on continental-margin slopes and ice-distal flanks of submarine moraine ridges, based on the presence of clear depositional sediment fronts and cross-cutting lobes on the flank. Where debris flows are observed, slope angles are very shallow (<2°), yet they have a run-out distance of over a kilometer. In shallow-slope settings, the ability of debris flows to achieve long run-out distances is considered possible through high-sediment-volume, low-viscosity behavior and excess sediment pore-water pressure [*Laberg and Vorren*, 1996; *Vorren and Werner*, 1998]. Sediment samples obtained from TMF settings typically contain a range of glacigenic sediments, consisting of muddy diamict, sands and gravels often with low shear strength and high water content. These properties reflect sediment delivery by subglacial deformation, ice-rafting and meltwater deposition in sediment laden plumes [*Kuvaas and Kristoffersen*, 1991; *Hambrey et al.*, 1992; *Laberg and Vorren*, 1996; *Dowdeswell et al.*, 2004]. Ice streaming over erodible, soft sedimentary beds has been suggested to be a prerequisite for the formation of TMFs

[*Ó Cofaigh et al.*, 2003]. High volumes of sediments suggested by debris flow deposits in Zone 2 therefore indicate the presence of a soft bed upstream of Jenkins Ridge.

The spherical mounds imaged in Zone 2 (Fig. 3k) are tentatively interpreted as subglacially-sourced boulders. Their dimensions (1-3 m in height and up to ~20 m in width) are large but within the upper limit of scales observed and considered theoretically possible to be transported subglacially [*Weertman*, 1958]. Crescent-shaped ridges bordering the boulders may have formed either by post-glacial accumulation of sediment during downslope sediment flow or âĂIJbulldozingâĂİ by the impact of the boulders striking the sea-bed following release from the base of the ice shelf. Adjacent linear scours (Fig. 3k) may have formed during debris avalanching down the ridge flank or could also be grounded-ice bedforms partially buried by proglacial sediments.

5.1.4 Bedforms of unknown genesis

The curvilinear ridges superimposed onto MSGLs in Zone 3, (left-hand zoom in Fig. 3i) extend transversally for about half the wavelength of the MSGLs, i.e. 300 m, from the trough of a MSGL to its crest. These ridges may be remnants of small-scale recessional moraines or alternatively, they may have formed by the lateral flow of a viscous basal ice layer between MSGL troughs and crests during grounded-ice-flow [*Schoof and Clarke*, 2008], or by postglacial current reworking of fine-grained surficial sediments.

Interpreting the genesis of the corrugation ridges overprinting the potential GZWs in Zone 4 (Fig. 4i) is also challenging. Formation by ephemeral grounding of sub-ice-shelf keels requires corrugation ridges to form on the lee slope of the potential GZW without scouring away its crest. It seems unlikely this would be possible through forward advection of ice keels. Squeezing of sediment ridges during grounding-line retreat could explain their location, but the surfaces of these corrugations have a weak acoustic signal in comparison to acoustic observations of recessional moraines in other studies [e.g. *Halberstadt et al.*, 2016]. Another possible mode of formation is through squeezing of sediment by basal crevasses. Regularly-spaced basal crevasses have been observed beneath the Larsen C [*Luckman et al.*, 2012] and Ross Ice shelves [*Jezek and Bentley*, 1983; *Anandakrishnan et al.*, 2007], however they typically have spacings at least an order of magnitude greater than the spacing of corrugations in Zone 3 (Fig. 4i). Acquisition of multibeam data in this region would enable a better assessment of their morphology and mode of formation.

5.2 Synthesis and implications

5.2.1 Key observations of the sub-ice shelf environment

The data interpreted above provide an unprecedented view of an ice stream bed that has been deglaciated within the past century. Based on our survey of the terrain, a number of important observations can be made that contribute to our wider understanding of these environments and to PIG specifically:

1. Sediment delivery from basal transport has played a key role in shaping each of the zones from the ice-shelf front to the modern grounding line. Our results suggest meltwater plumes and rainout have been important to the accumulation of ice-distal sediments in small basins seaward of the ice shelf. Indeed, observations through Zones 2-4 demonstrate that till deposition and secondary reworking of till (via mass movement to produce debris flows) are the dominant sediment producing and landform-generating processes in this recently deglaciated cavity.
2. Beneath PIGIS, changes in bed properties, specifically contrasting scales of lineations, occur abruptly over limited geographic areas of the bed (Fig. 5). This finding supports the relatively small number of ice-stream bed studies that have presented similar evidence for highly variable basal conditions beneath Antarctic ice streams [e.g. *Smith and Murray*, 2009; *Smith et al.*, 2013]. However, rather than showing zones of stiff till with no bedforms contrasting with zones of soft till with lineations [*King et al.*, 2009], we are able to show variability in bedforms within a region where sediment cores indicate the presence of deformable sediment [*Smith et al.*, 2017].
3. Grounding by sub-ice-shelf keels is a process that appears to produce significant features near the grounding zone (e.g. erosional scours). This process may be responsible for the appearance of converging lineations observed in regions of elevated seafloor (e.g., Fig. 3j). These variations suggest a more mobile grounding situation in some parts of the ridge, such as might be expected in an ice-plain environment [*Corr et al.*, 2001].
4. Former-ice-flow-oriented lineations on a scale intermediate between MSGL and flutes can form at the grounding zones of major ice streams, and cross-cutting generations at the margins preserve a record of localized flow variability.

5. The presence of glacitectonic rafts and emplaced boulders indicate that till deformation may not be the only sediment transport process in operation under West Antarctic ice streams, and that plucking and rafting of large bedrock/sediment blocks contributes to erosion beneath PIG.
6. The landform mapping presented in this study shows a transition from bedrock outcrops in Zone 1 to sediment bedforms and deposits in Zone 2 broadly coincident with the crystalline to sedimentary bed transition inferred from aerogravity surveys [*Muto et al.*, 2013, 2016]. These surveys inferred a thick sedimentary basin extending upstream of the grounding line that would provide an abundant source for sediments deposited as mass flows, MSGL and GZWs in Zones 2-4. These observations indicate that Jenkins Ridge marks a transition between hard, resistant crystalline bedrock to more erodible, soft sedimentary bed upstream of the present-day grounding line. Such transitions have been observed further seaward on the continental shelf and associated with contrasts in the distribution of sediment and character of geomorphic features [*Lowe and Anderson*, 2002; *Wellner et al.*, 2001, 2006; *Graham et al.*, 2009].

5.2.2 Observations of fine-scale bedforms: preservation or data resolution?

High-resolution imaging of the seafloor beneath PIGIS reveals a complex pattern of landforms indicative of a highly dynamic environment. We have identified seldom observed fine-scale submarine landforms, namely curvilinear sediment ridges, intermediate-scale lineations and small-scale hill-hole pairs. With the exception of lineations, these landforms are interpreted as reworked subglacial bedforms, sculpted into their present form by overriding of the ice margin and sub-ice-shelf keels during retreat of the grounding-line. We consider the ability to detect these features is a factor of 1) the youth of the sub-ice-shelf landscape and 2) the high resolution of the data compared to offshore swath bathymetric surveying.

Smith et al. [2017] calculated sedimentation rates on the crest of Jenkins Ridge (Zone 3) of 0.82-0.95 mm a^{-1}. These rates are too low to have buried the fine-scale features such as curvilinear sediment ridges and sub-metre amplitude lineations since ungrounding from the ridge crest in 1940. Further seaward on the continental shelf, features of this scale may not be as well preserved having been exposed to marine sedimentation for up to several millennia. However, deep-tow side-scan sonar surveys of the continental shelf have revealed fine-scale landforms such as flutes and corrugations (“washboard pattern”) located near the continental shelf break [*Lien and Rokoengen*, 1989; *Ship et al.*, 1999; *Shipp et al.*, 2002].

The identification of fine-scale features may therefore be primarily a factor of the ability to image the seafloor at sub-metre to metre-scale resolution. We demonstrate this in Figure 6 by conducting a crossover comparison between AUV and ship-based multibeam surveys in Pine Island Bay [*Nitsche et al.*, 2013], just seaward of PIGIS. This analysis reveals intermediate-scale lineations overprinting MSGL, and demonstrates the preservation of fine-scale bedforms ~85 km in front of the modern grounding-line (Fig. 6). Our data indicate there is likely a wealth of detailed information of glacial processes not captured by standard offshore marine geophysical surveys. Recent work by *García et al.* [2016] using a remotely-operated underwater vehicle also illustrate the level of detail obtained using these methods. Further targeted AUV/ROV surveys beneath ice shelves and on the continental shelf would provide useful information on bedform preservation and may elucidate processes related to some of the more enigmatic landforms observed beneath PIGIS.

Figure 6. Comparison of offshore swath bathymetry and Autosub3 multibeam bathymetry. a, 35 m resolution swath sonar bathymetry of Pine Island Bay acquired offshore seaward of PIGIS [Data from *Nitsche et al.*, 2013] overlain by Autosub3 bathymetry from Mission M433 at 2 m resolution (red polygon). **b**, Magnified image showing the difference in detail between datasets. Large black arrows mark the locations of MSGL visible on both the offshore swath sonar and Autosub3 multibeam bathymetry, small-black arrows denote intermediate-scale lineations only visible on the Autosub3 bathymetry data. Location of data extent is shown in Figure 1a.

6 Conclusions

We have used high-resolution bathymetry and sub-bottom-profiler data obtained by AUV surveys to explore the nature of seafloor bedforms and sediment properties beneath a recently ungrounded Antarctic ice shelf. These data reveal fine-scale landforms in a dynamic environment modified by subglacial erosion, meltwater flow, and sediment deposition, providing an unprecedented view of a recently deglaciated ice-stream bed.

The landscape and sediments we have imaged beneath Pine Island Glacier Ice Shelf record features of direct subglacial erosion and deposition, and postglacial modification by overriding and scouring of ice-shelf keels and gravity-driven slope processes. Seaward of Jenkins Ridge the landscape of streamlined bedrock outcrops is characteristic of direct subglacial erosion with little postglacial modification. In this landscape, ice-rafted boulders, hill-hole pairs and glacitectonic rafts indicate that freeze-on and plucking of basal material is a significant component of erosion and sediment transport. Upstream over Jenkins Ridge and into the sub-ice-shelf cavity, the landscape is draped by sediments which evince both direct glacial deposition and deformation, and post-glacial modification. This sediment distribution supports Jenkins Ridge having been a stable grounding-line location for a significant period prior to its 20th-century ungrounding.

We have demonstrated the value of imaging recently deglaciated terrain at meter-scale resolution. The insights we have provided through the analysis of fine-scale landforms would not have been achievable without the capability to observe features in recently deglaciated and at meter-scale resolution using an AUV platform. Such landforms are likely to be rapidly modified by postglacial sedimentation or are not readily observable in coarser resolution swath bathymetry datasets.

We recommend further AUV missions to sub-ice shelf cavities to enable a better understanding of recent controls on ice stream retreat and sub-ice shelf processes. Surveys of selected offshore regions previously covered by offshore swath bathymetry surveys would also provide a clearer picture of past ice stream stability and retreat.

Acknowledgments

This work was supported by funding from the UK Natural Environment Research Council (NERC) iSTAR Programme Grants NE/J005665/2 and NE/J005770/1 and NERC Grant NE/G001367/1. DD was supported by NERC Training Grant NE/K011189/1. FON was supported by NSF grant ANT-838735. MS was supported by NERC Grant NE/J004766/1. AJ We thank the Autosub technical teams led by Steve McPhail and the Captain and cruise participants of RRS James Clark Ross cruise JR294/295 and RVIB Nathaniel B Palmer cruise NBP09-01 for conducting the AUV operations. We thank Julian Dowdeswell and two anonymous reviewers for constructive reviews which improved the clarity of the manuscript. Data used in this article can be obtained from the UK Polar Data Centre.

References

Alley, R., K. Cuffey, E. Evenson, J. Strasser, D. Lawson, and G. Larson (1997), How glaciers entrain and transport basal sediment: Physical constraints, *Quaternary Science Reviews*, *16*(9), 1017 – 1038, doi:http://dx.doi.org/10.1016/S0277-3791(97)00034-6.

Amblas, D., R. Urgeles, M. Canals, A. M. Calafat, M. Rebesco, A. Camerlenghi, F. Estrada, M. De Batist, and J. E. Hughes-Clarke (2006), Relationship between continental rise development and palaeo-ice sheet dynamics, Northern Antarctic Peninsula Pacific margin, *Quaternary Science Reviews*, *25*(9), 933–944, doi: 10.1016/j.quascirev.2005.07.012.

Anandakrishnan, S., G. a. Catania, R. B. Alley, and H. J. Horgan (2007), Discovery of till deposition at the grounding line of Whillans Ice Stream., *Science*, *315*(5820), 1835–1838, doi:10.1126/science.1138393.

Anderson, J. B., S. S. Shipp, A. L. Lowe, J. S. Wellner, and A. B. Mosola (2002), The Antarctic Ice Sheet during the Last Glacial Maximum and its subsequent retreat history: a review, *Quaternary Science Reviews*, *21*(1ÃćâĆňâĂIJ3), 49 – 70, {EPILOG}.

Anderson, J. B., H. Conway, P. J. Bart, A. E. Witus, S. L. Greenwood, R. M. McKay, B. L. Hall, R. P. Ackert, K. Licht, M. Jakobsson, and J. O. Stone (2014), Ross Sea paleo-ice sheet drainage and deglacial history during and since the LGM, *Quaternary Science Reviews*, *100*, 31 – 54, doi:http://dx.doi.org/10.1016/j.quascirev.2013.08.020.

Andreassen, K., L. C. Nilssen, B. Rafaelsen, and L. Kuilman (2004), Three-dimensional seismic data from the Barents Sea margin reveal evidence of past ice streams and their dynamics, *Geology*, *32*(8), 729–732.

Batchelor, C. L., J. A. Dowdeswell, and K. A. Hogan (2011), Late Quaternary ice flow and sediment delivery through Hinlopen Trough, Northern Svalbard margin: Submarine landforms and depositional fan, *Marine Geology*, *284*(1-4), 13–27, doi: 10.1016/j.margeo.2011.03.005.

Bingham, R. G., F. Ferraccioli, E. C. King, R. D. Larter, H. D. Pritchard, A. M. Smith, and D. G. Vaughan (2012), Inland thinning of West Antarctic Ice Sheet steered along subglacial rifts, *Nature*, *487*(7408), 468–471.

Brisbourne, A. M., A. M. Smith, D. G. Vaughan, E. C. King, D. Davies, R. G. Bingham, E. C. Smith, I. J. Nias, and S. H. R. Rosier (2017), Bed conditions of Pine Island Glacier, West Antarctica, *Journal of Geophysical Research: Earth Surface*, *122*(1), 419–433, doi:10.1002/2016JF004033, 2016JF004033.

Clark, C. D. (1993), Mega-scale glacial lineations and cross-cutting ice-flow landforms, *Earth Surface Processes and Landforms*, *18*(1), 1–29, doi:10.1002/esp.3290180102.

Corr, H. F. J., C. S. M. Doake, A. Jenkins, and D. G. Vaughan (2001), Investigations of an “ice plain" in the mouth of Pine Island Glacier, Antarctica, *Journal of Glaciology*, *47*(156), 51–57, doi:Doi 10.3189/172756501781832395.

Damuth, J. E. (1978), Echo character of the Norwegian-Greenland Sea: Relationship to Quaternary sedimentation, *Marine Geology*, *28*(1-2), 1–36, doi:10.1016/0025-3227(78)90094-4.

Domack, E., D. Duran, A. Leventer, S. Ishman, et al. (2005), Stability of the larsen b ice shelf on the antarctic peninsula during the holocene epoch, *Nature*, *436*(7051), 681.

Dowdeswell, J., and J. Bamber (2007), Keel depths of modern Antarctic icebergs and implications for sea-floor scouring in the geological record, *Marine Geology*, *243*(1ÃćâĆňâĂIJ4), 120 – 131, doi:http://dx.doi.org/10.1016/j.margeo.2007.04.008.

Dowdeswell, J., A. Elverhøi, and R. Spielhagen (1998), Glacimarine sedimentary processes and facies on the polar North Atlantic margins., *Quaternary Science Reviews*, *17*(1), 243–272, doi:10.1016/S0277-3791(97)00071-1.

Dowdeswell, J., C. Ó Cofaigh, and C. Pudsey (2004), Continental slope morphology and sedimentary processes at the mouth of an Antarctic palaeo-ice stream, *Marine Geology*, *204*(1), 203–214, doi:10.1016/S0025-3227(03)00338-4.

Dowdeswell, J. A., J. Evans, R. Mugford, G. Griffiths, S. McPhail, N. Millard, P. Stevenson, M. A. Brandon, C. Banks, K. J. Heywood, M. R. Price, P. A. Dodd, A. Jenkins, K. W. Nicholls, D. Hayes, E. P. Abrahamsen, P. Tyler, B. Bett, D. Jones, P. Wadhams, J. P. Wilkinson, K. Stansfield, and S. Ackley (2008), Autonomous underwater vehicles (AUVs) and investigations of the ice-ocean interface in Antarctic and Arctic waters, *Journal of Glaciology*, *54*(187), 661–672, doi:10.3189/002214308786570773.

Dowdeswell, J. A., D. Ottesen, and L. Plassen (2016), Debris-flow lobes on the distal flanks of terminal moraines in spitsbergen fjords, *Geological Society, London, Memoirs*, *46*(1), 77–78, doi:10.1144/M46.97.

Dupont, T. K., and R. B. Alley (2005), Assessment of the importance of ice-shelf buttressing to ice-sheet flow, *Geophysical Research Letters*, *32*(4), n/a–n/a, doi: 10.1029/2004GL022024, l04503.

Dutrieux, P., J. De Rydt, A. Jenkins, P. R. Holland, H. K. Ha, S. H. Lee, E. J. Steig, Q. Ding, E. P. Abrahamsen, and M. Schröder (2014a), Strong sensitivity of Pine Island ice-shelf melting to climatic variability, *Science*, *343*(6167), 174–178.

Dutrieux, P., C. Stewart, A. Jenkins, K. W. Nicholls, H. F. J. Corr, E. Rignot, and K. Steffen (2014b), Basal terraces on melting ice shelves, *Geophysical Research Letters*, *41*(15), 5506–5513, doi:10.1002/2014GL060618, 2014GL060618.

Fürst, J. J., G. Durand, F. Gillet-chaulet, L. Tavard, M. Rankl, M. Braun, and O. Gagliardini (2016), The safety band of Antarctic ice shelves, *6*(May), 2014–2017, doi: 10.1038/NCLIMATE2912.

Gales, J. A., R. D. Larter, and P. T. Leat (2016), Iceberg ploughmarks and associated sediment ridges on the southern weddell sea margin, *Geological Society, London, Memoirs*, *46*(1), 289–290, doi:10.1144/M46.11.

García, M., J. A. Dowdeswell, R. Noormets, K. Hogan, J. Evans, C. Ó. Cofaigh, and R. D. Larter (2016), Geomorphic and shallow-acoustic investigation of an antarctic peninsula fjord system using high-resolution rov and shipboard geophysical observations: Ice dynamics and behaviour since the last glacial maximum, *Quaternary Science Reviews*, *153*, 122–138.

Graham, A. G. C., R. D. Larter, K. Gohl, C.-D. Hillenbrand, J. A. Smith, and G. Kuhn (2009), Bedform signature of a West Antarctic palaeo-ice stream reveals a multi-temporal record of flow and substrate control, *Quaternary Science Reviews*, *28*(25-26), 2774–2793.

Graham, A. G. C., R. D. Larter, K. Gohl, J. A. Dowdeswell, C.-D. Hillenbrand, J. A. Smith, J. Evans, G. Kuhn, and T. Deen (2010), Flow and retreat of the Late Quaternary Pine Island-Thwaites palaeo-ice stream, West Antarctica, *Journal of Geophysical Research*, *115*(F3).

Graham, A. G. C., P. Dutrieux, D. G. Vaughan, F. O. Nitsche, R. Gyllencreutz, S. L. Greenwood, R. D. Larter, and A. Jenkins (2013), Seabed corrugations beneath an Antarctic ice shelf revealed by autonomous underwater vehicle survey: Origin and implications for the history of Pine Island Glacier, *Journal of Geophysical Research: Earth Surface*, *118*(3), 1356–1366, doi:10.1002/jgrf.20087.

Halberstadt, A. R. W., L. M. Simkins, S. L. Greenwood, and J. B. Anderson (2016), Past ice-sheet behaviour: Retreat scenarios and changing controls in the Ross Sea, Antarctica, *Cryosphere*, *10*(3), 1003–1020, doi:10.5194/tc-10-1003-2016.

Hambrey, M. J., W. U. Ehrmann, and B. Larsen (1992), *Cenozoic glacial record of the Prydz Bay continental shelf, East Antarctica*, Geological Survey in Denmark.

Hillenbrand, C.-D., J. A. Smith, D. A. Hodell, M. Greaves, C. R. Poole, S. Kender, M. Williams, T. J. Andersen, P. E. Jernas, H. Elderfield, et al. (2017), West antarctic ice sheet retreat driven by holocene warm water incursions, *Nature*, *547*(7661), 43–48.

Hogan, K. A., J. A. Dowdeswell, and C. Ó Cofaigh (2012), Glacimarine sedimentary processes and depositional environments in an embayment fed by West Greenland ice streams, *Marine Geology*, *311-314*, 1–16, doi:10.1016/j.margeo.2012.04.006.

Hurst, M. D., S. M. Mudd, R. Walcott, M. Attal, and K. Yoo (2012), Using hilltop curvature to derive the spatial distribution of erosion rates, *Journal of Geophysical Research: Earth Surface*, *117*(F2), n/a–n/a, doi:10.1029/2011JF002057, f02017.

Jacobs, S. S., H. H. Hellmer, and A. Jenkins (1996), Antarctic ice sheet melting in the southeast Pacific, *Geophysical Research Letters*, *23*(9), 957–960, doi: 10.1029/96GL00723.

Jacobs, S. S., A. Jenkins, C. F. Giulivi, and P. Dutrieux (2011), Stronger ocean circulation and increased melting under Pine Island Glacier ice shelf, *Nature Geosci*, *4*, 519–523.

Jakobsson, M., J. B. Anderson, F. O. Nitsche, J. A. Dowdeswell, R. Gyllencreutz, N. Kirchner, R. Mohammad, M. O'Regan, R. B. Alley, S. Anandakrishnan, B. Eriksson, A. Kirshner, R. Fernandez, T. Stolldorf, R. Minzoni, and W. Majewski (2011), Geological record of ice shelf break-up and grounding line retreat, Pine Island Bay, West Antarctica, *Geology*, *39*(7), 691–694, doi:10.1130/G32153.1.

Jenkins, A., P. Dutrieux, S. S. Jacobs, S. D. McPhail, J. R. Perrett, A. T. Webb, and D. White (2010), Observations beneath Pine Island Glacier in West Antarctica and implications for its retreat, *Nature Geosci*, *3*, 468–472.

Jezek, K. C., and C. R. Bentley (1983), Field studies of bottom crevasses in the Ross Ice Shelf, Antarctica, *Journal of Glaciology*, *29*(101), 118–126.

Jordan, T. A., F. Ferraccioli, D. G. Vaughan, J. W. Holt, H. Corr, D. D. Blankenship, and T. M. Diehl (2009), Aerogravity evidence for major crustal thinning under the Pine Island Glacier region (West Antarctica), *Geological Society of America Bulletin*, *122*(5-6), 714–726.

Joughin, I., D. E. Shean, B. E. Smith, and P. Dutrieux (2016), Grounding line variability and subglacial lake drainage on Pine Island Glacier, Antarctica, *Geophysical Research Letters*, *43*(17), 9093–9102, doi:10.1002/2016GL070259, 2016GL070259.

King, E. C., R. C. A. Hindmarsh, and C. R. Stokes (2009), Formation of mega-scale glacial lineations observed beneath a West Antarctic ice stream, *Nature Geosci*, *2*, 585–

588.

Konrad, H., L. Gilbert, S. L. Cornford, A. Payne, A. Hogg, A. Muir, and A. Shepherd (2017), Uneven onset and pace of ice-dynamical imbalance in the Amundsen Sea Embayment, West Antarctica, *Geophysical Research Letters*, pp. 910–918, doi: 10.1002/2016GL070733, 2016GL070733.

Kuvaas, B., and Y. Kristoffersen (1991), The Crary Fan: a trough-mouth fan on the Weddell Sea continental margin, Antarctica, *Marine Geology*, *97*(3-4), 345–362.

Laberg, J., and T. O. Vorren (1996), Late Weichselian submarine debris flow deposits on the Bear Island Trough Mouth Fan, *Oceanographic Literature Review*, *43*(4), 368.

Lien, S. A. E. A., R, and K. Rokoengen (1989), Iceberg scouring and sea bed morphology on the eastern weddell sea shelf, antarctica, *Polar Research*, *7*(1), 43–57, doi: 10.1111/j.1751-8369.1989.tb00603.x.

Lowe, A. L., and J. B. Anderson (2002), Reconstruction of the West Antarctic Ice Sheet in Pine Island Bay during the Last Glacial Maximum and its subsequent retreat history, *Quaternary Science Reviews*, *21*(16ÃćâĆňâĂIJ17), 1879 – 1897.

Luckman, A., D. Jansen, B. Kulessa, E. C. King, P. Sammonds, and D. I. Benn (2012), The Cryosphere Basal crevasses in Larsen C Ice Shelf and implications for their global abundance, pp. 113–123, doi:10.5194/tc-6-113-2012.

LysÃě, A., B. Hjelstuen, and E. Larsen (2010), Fjord infill in a high-relief area: Rapid deposition influenced by deglaciation dynamics, glacio-isostatic rebound and gravitational activity, *Boreas*, *39*(1), 39–55, doi:10.1111/j.1502-3885.2009.00117.x.

McMillan, M., A. Shepherd, A. Sundal, K. Briggs, A. Muir, A. Ridout, A. Hogg, and D. Wingham (2014), Increased ice losses from Antarctica detected by CryoSat-2, *Geophysical Research Letters*, *41*(11), 3899–3905, doi:10.1002/2014GL060111, 2014GL060111.

McPhail, S. (2009), Autosub6000: A Deep Diving Long Range AUV, *Journal of Bionic Engineering*, *6*(1), 55 – 62, doi:http://dx.doi.org/10.1016/S1672-6529(08)60095-5.

McPhail, S. D., M. E. Furlong, M. Pebody, J. R. Perrett, P. Stevenson, A. Webb, and D. White (2009), Exploring beneath the PIG Ice Shelf with the Autosub3 AUV, in *OCEANS 2009-EUROPE*, pp. 1–8, doi:10.1109/OCEANSE.2009.5278170.

Moran, S., L. Clayton, R. Hooke, M. Fenton, and L. Andriashek (1980), Glacier-bed landforms of the prairie region of North America., *Journal of Glaciology*, *25*(93), 457–476, cited By 92.

Mouginot, J., E. Rignot, and B. Scheuchl (2014), Sustained increase in ice discharge from the Amundsen Sea Embayment, West Antarctica, from 1973 to 2013, *Geophysical Research Letters*, *41*(5), 1576–1584.

Muto, A., S. Anandakrishnan, and R. B. Alley (2013), Subglacial bathymetry and sediment layer distribution beneath the Pine Island Glacier ice shelf, West Antarctica, modeled using aerogravity and autonomous underwater vehicle data, *Annals of Glaciology*, *54*(64), 27–32, doi:10.3189/2013AoG64A110.

Muto, A., L. E. Peters, K. Gohl, I. Sasgen, R. B. Alley, S. Anandakrishnan, and K. L. Riverman (2016), Subglacial bathymetry and sediment distribution beneath Pine Island Glacier ice shelf modeled using aerogravity and in situ geophysical data: New results, *Earth and Planetary Science Letters*, *433*, 63–75, doi:10.1016/j.epsl.2015.10.037.

Nicholls, K. W., E. P. Abrahamsen, J. J. H. Buck, P. A. Dodd, C. Goldblatt, G. Griffiths, K. J. Heywood, N. E. Hughes, A. Kaletzky, G. F. Lane-Serff, S. D. McPhail, N. W. Millard, K. I. C. Oliver, J. Perrett, M. R. Price, C. J. Pudsey, K. Saw, K. Stansfield, M. J. Stott, P. Wadhams, A. T. Webb, and J. P. Wilkinson (2006), Measurements beneath an Antarctic ice shelf using an autonomous underwater vehicle, *Geophysical Research Letters*, *33*(8), n/a–n/a, doi:10.1029/2006GL025998, l08612.

Nitsche, F. O., K. Gohl, R. D. Larter, C.-D. Hillenbrand, G. Kuhn, J. A. Smith, S. Jacobs, J. B. Anderson, and M. Jakobsson (2013), Paleo ice flow and subglacial meltwater dynamics in Pine Island Bay, West Antarctica, *The Cryosphere*, *7*(1), 249–262.

Ó Cofaigh, C. Ã., J. Taylor, J. A. Dowdeswell, and C. J. Pudsey (2003), Palaeo-ice streams, trough mouth fans and high-latitude continental slope sedimentation, *Boreas*, *32*(1), 37–55.

Ottesen, D., and J. Dowdeswell (2006), Assemblages of submarine landforms produced by tidewater glaciers in svalbard, *Journal of Geophysical Research: Earth Surface*, *111*(F1).

Ottesen, D., C. R. Stokes, R. BÃČÂÿe, L. Rise, O. Longva, T. Thorsnes, O. Olesen, T. Bugge, A. Lepland, and O. B. Hestvik (2016), Landform assemblages and sedimentary processes along the Norwegian Channel Ice Stream, *Sedimentary Geology*, *338*, 115 – 137, doi:http://dx.doi.org/10.1016/j.sedgeo.2016.01.024.

Paolo, F. S., H. A. Fricker, and L. Padman (2015), Volume loss from Antarctic ice shelves is accelerating, *Science*, *348*(6232), 327–331, doi:10.1126/science.aaa0940.

Park, J. W., N. Gourmelen, A. Shepherd, S. W. Kim, D. G. Vaughan, and D. J. Wingham (2013), Sustained retreat of the Pine Island Glacier, *Geophysical Research Letters*, *40*(10), 2137–2142.

Pritchard, H. D., S. R. Ligtenberg, H. A. Fricker, D. G. Vaughan, M. R. van den Broeke, and L. Padman (2012), Antarctic ice-sheet loss driven by basal melting of ice shelves, *Nature*, *484*(7395), 502–5.

Rebesco, M., Y. Liu, A. Camerlenghi, M. Winsborrow, J. S. Laberg, A. Caburlotto, P. Diviacco, D. Accettella, C. Sauli, N. Wardell, and I. Tomini (2011), Deglaciation of the western margin of the Barents Sea Ice Sheet. A swath bathymetric and sub-bottom seismic study from the Kveithola Trough, *Marine Geology*, *279*(1-4), 141–147.

Rignot, E., D. G. Vaughan, M. Schmeltz, T. Dupont, and D. MacAyeal (2002), Acceleration of Pine Island and Thwaites Glaciers, West Antarctica, *Annals of Glaciology*, *34*, 189–194, doi:10.3189/172756402781817950.

Rignot, E., J. L. Bamber, M. R. van den Broeke, C. Davis, Y. Li, W. J. van de Berg, and E. van Meijgaard (2008), Recent Antarctic ice mass loss from radar interferometry and regional climate modelling, *Nature Geoscience*, *1*(2), 106–110.

Rignot, E., I. Velicogna, M. R. van den Broeke, A. Monaghan, and J. T. M. Lenaerts (2011), Acceleration of the contribution of the Greenland and Antarctic ice sheets to sea level rise, *Geophysical Research Letters*, *38*(5), n/a–n/a, doi:10.1029/2011GL046583.

Rignot, E., S. Jacobs, J. Mouginot, and B. Scheuchl (2013), Ice-shelf melting around Antarctica, *Science*, *341*(6143), 266–270, doi:10.1126/science.1235798.

Rignot, E., J. Mouginot, M. Morlighem, H. Seroussi, and B. Scheuchl (2014), Widespread, rapid grounding line retreat of Pine Island, Thwaites, Smith, and Kohler glaciers, West Antarctica, from 1992 to 2011, *Geophysical Research Letters*, *41*(10), 3502–3509.

Rüther, D., K. Andreassen, and M. Spagnolo (2013), Aligned glaciotectonic rafts on the central Barents Sea seafloor revealing extensive glacitectonic erosion during the last deglaciation, *Geophysical Research Letters*, *40*(24), 6351–6355, doi:10.1002/2013GL058413, 2013GL058413.

Rüther, D. C., K. Andreassen, and M. Spagnolo (2016), Aligned glacitectonic rafts on the floor of the central Barents Sea, *Geological Society, London, Memoirs*, *46*(1), 189 LP – 190.

Schoof, C. G., and G. K. C. Clarke (2008), A model for spiral flows in basal ice and the formation of subglacial flutes based on a Reiner-Rivlin rheology for glacial ice, *Journal of Geophysical Research*, *113*(B5).

Scott, J. B. T., G. H. Gudmundsson, A. M. Smith, R. G. Bingham, H. D. Pritchard, and D. G. Vaughan (2009), Increased rate of acceleration on Pine Island Glacier strongly coupled to changes in gravitational driving stress, *The Cryosphere*, *3*, 125–131, doi: doi:10.5194/tc-3-125-2009.

Ship, S., J. Anderson, and E. Domack (1999), Late Pleistocene–Holocene retreat of the West Antarctic Ice-Sheet system in the Ross Sea: part 1âĂŤgeophysical results, *Geological Society of America Bulletin*, *111*(10), 1486–1516.

Shipp, S., J. Anderson, and E. Domack (1999), Late Pleistocene-Holocene retreat of the West Antarctic Ice-Sheet system in the Ross Sea: Part 1 - geophysical results, *Bulletin of the Geological Society of America*, *111*(10), 1486–1516, cited By 241.

Shipp, S. S., J. S. Wellner, and J. B. Anderson (2002), Retreat signature of a polar ice stream: sub-glacial geomorphic features and sediments from the Ross Sea, Antarctica, *Geological Society, London, Special Publications*, *203*(1), 277–304, doi: 10.1144/GSL.SP.2002.203.01.15.

Simkins, L. M., J. B. Anderson, and S. L. Greenwood (2016), Glacial landform assemblage reveals complex retreat of grounded ice in the ross sea, antarctica, *Geological Society, London, Memoirs*, *46*(1), 353–356, doi:10.1144/M46.168.

Smith, A. M., and T. Murray (2009), Bedform topography and basal conditions beneath a fast-flowing West Antarctic ice stream, *Quaternary Science Reviews*, *28*(7-8), 584–596.

Smith, A. M., T. A. Jordan, F. Ferraccioli, and R. G. Bingham (2013), Influence of subglacial conditions on ice stream dynamics: Seismic and potential field data from Pine Island Glacier, West Antarctica, *Journal of Geophysical Research: Solid Earth*, *118*(4), 1471–1482.

Smith, J. A., T. J. Andersen, M. Shortt, A. M. Gaffney, M. Truffer, T. P. Stanton, R. Bindschadler, P. Dutrieux, A. Jenkins, C. Hillenbrand, W. Ehrmann, H. F. J. Corr, N. Farley, S. Crowhurst, and D. G. Vaughan (2017), Sub-ice-shelf sediments record history of twentieth-century retreat of Pine Island Glacier, *Nature*, *541*(7635), 77–80, doi: 10.1038/nature20136.

Smith, M. J., and C. D. Clark (2005), Methods for the visualization of digital elevation models for landform mapping, *Earth Surface Processes and Landforms*, *30*(7), 885–900.

Spagnolo, M., C. D. Clark, J. C. Ely, C. R. Stokes, J. B. Anderson, K. Andreassen, A. G. C. Graham, and E. C. King (2014), Size, shape and spatial arrangement of mega-scale glacial lineations from a large and diverse dataset, *Earth Surface Processes and*

Landforms, *39*(11), 1432–1448, doi:10.1002/esp.3532.

Studinger, M., C. Allen, W. Blake, L. Shi, S. Elieff, W. Krabill, J. Sonntag, S. Martin, P. Dutrieux, A. Jenkins, et al. (2010), Mapping pine island glacier's sub-ice cavity with airborne gravimetry, in *AGU Fall Meeting Abstracts*.

Turner, J., A. Orr, G. H. Gudmundsson, A. Jenkins, R. G. Bingham, C.-D. Hillenbrand, and T. J. Bracegirdle (2017), Atmosphere-ocean-ice interactions in the Amundsen Sea Embayment, West Antarctica, *Reviews of Geophysics*, pp. n/a–n/a, doi: 10.1002/2016RG000532, 2016RG000532.

Vorren, L. J. B. F. D. J. K. N. M. J. R. J., T., and F. Werner (1998), The Norwegian-Greenland Sea continental margins: morphology and Late Quaternary sedimentary processes and environment., *Quaternary Science Reviews*, *17*(1), 273 – 302, doi: http://dx.doi.org/10.1016/S0277-3791(97)00072-3.

Weertman, J. (1958), Transport of boulders by glaciers and ice sheets, *International Association of Scientific Hydrology Bulletin*, *3*(2), 44–44, doi:10.1080/02626665809493102.

Wellner, J., A. Lowe, S. Shipp, and J. Anderson (2001), Distribution of glacial geomorphic features on the Antarctic continental shelf and correlation with substrate: implications for ice behavior, *Journal of Glaciology*, *47*(158), 397–411, doi: doi:10.3189/172756501781832043.

Wellner, J., D. Heroy, and J. Anderson (2006), The death mask of the antarctic ice sheet: Comparison of glacial geomorphic features across the continental shelf, *Geomorphology*, *75*(1ÃćâĆňâĂIJ2), 157 – 171, doi: http://dx.doi.org/10.1016/j.geomorph.2005.05.015.

Wingham, D. J., D. W. Wallis, and A. Shepherd (2009), Spatial and temporal evolution of Pine Island Glacier thinning, 1995âĂŞ2006, *Geophysical Research Letters*, *36*(17), doi:10.1029/2009GL039126, l17501.

Wynn, R. B., V. A. I. Huvenne, T. P. Le Bas, B. J. Murton, D. P. Connelly, B. J. Bett, H. A. Ruhl, K. J. Morris, J. Peakall, D. R. Parsons, E. J. Sumner, S. E. Darby, R. M. Dorrell, and J. E. Hunt (2014), Autonomous Underwater Vehicles (AUVs): Their past, present and future contributions to the advancement of marine geoscience, *Marine Geology*, *352*, 451–468, doi:10.1016/j.margeo.2014.03.012.

Figure 1.

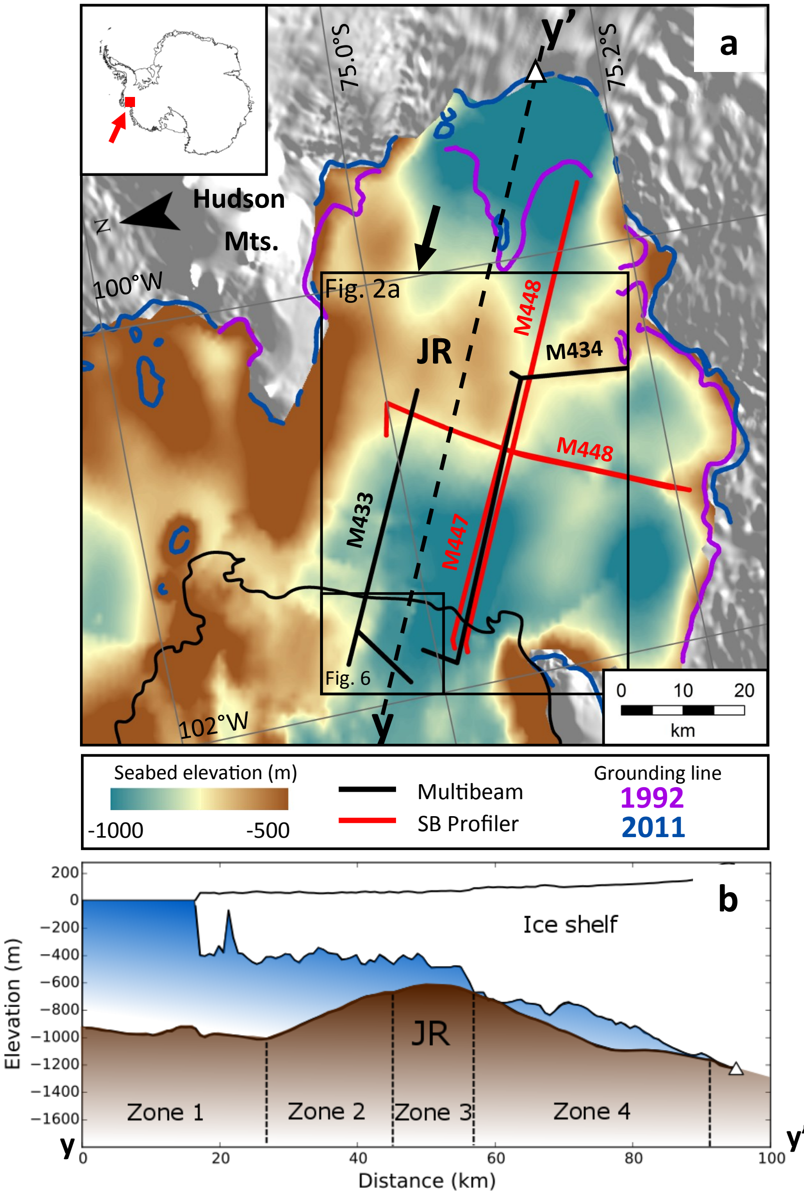

a
75.0°S
75.2°S
y'
N
Hudson
Mts.
100°W
Fig. 2a
JR
M448
M434
M448
M433
M447
Fig. 6
102°W
y
0 10 20
km
Seabed elevation (m)
-1000
-500
Multibeam
SB Profiler
Grounding line
1992
2011
b
Ice shelf
JR
Zone 1
Zone 2
Zone 3
Zone 4
Elevation (m)
Distance (km)
y
y'

Figure 2.

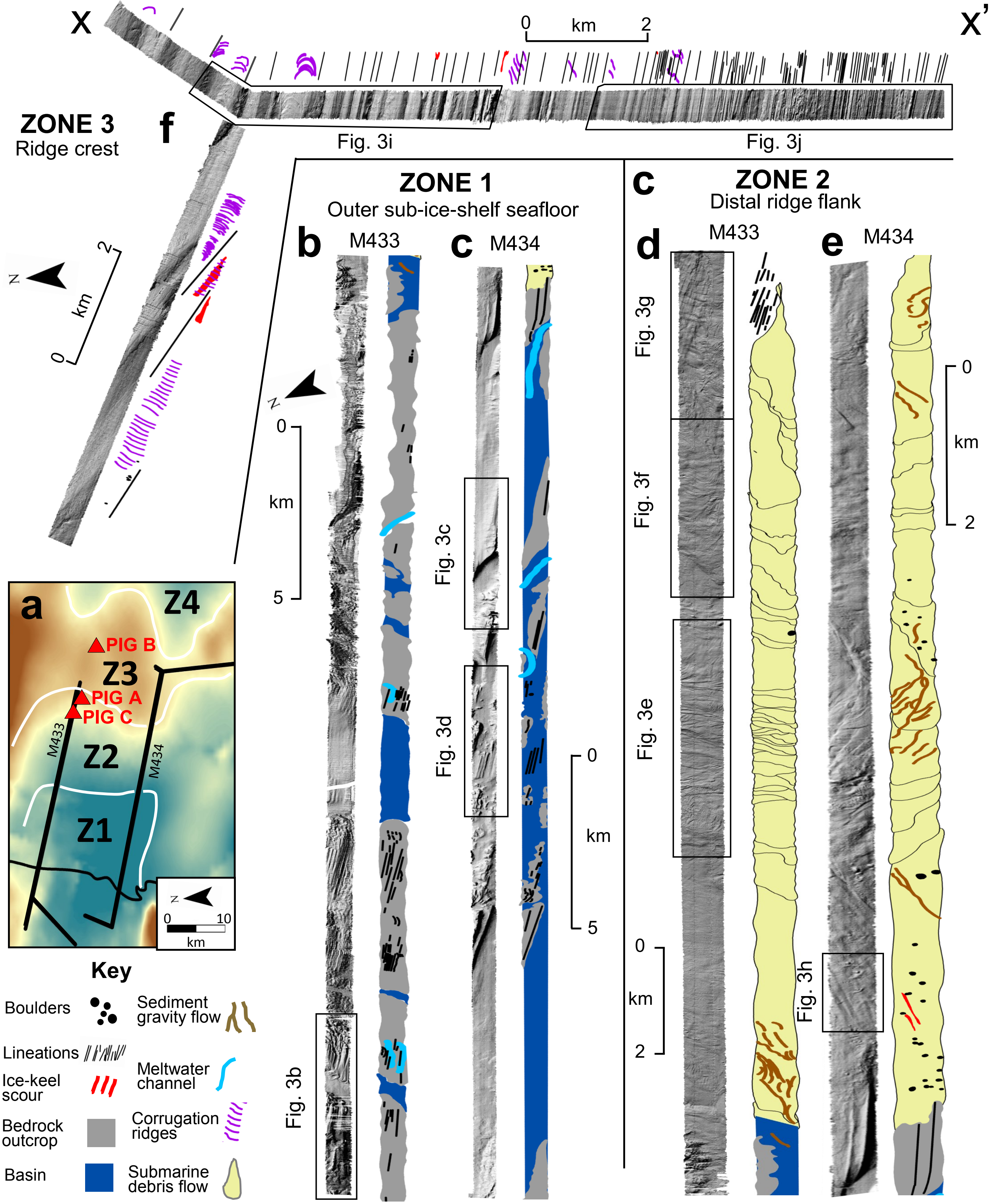
X
X'
0 km 2
ZONE 3
Ridge crest
f
Fig. 3i
Fig. 3j
N
0 km 2
ZONE 1
Outer sub-ice-shelf seafloor
b M433
c M434
0 km 5
Fig. 3c
Fig. 3d
Fig. 3b
0 km 5
c
ZONE 2
Distal ridge flank
d M433
e M434
Fig. 3g
Fig. 3f
Fig. 3e
0 km 2
Fig. 3h
0 km 2
a
Z4
PIG B
Z3
PIG A
PIG C
Z2
Z1
M433
M434
N
0 10
km
Key
Boulders
Sediment gravity flow
Lineations
Ice-keel scour
Meltwater channel
Bedrock outcrop
Corrugation ridges
Basin
Submarine debris flow

Figure 3.

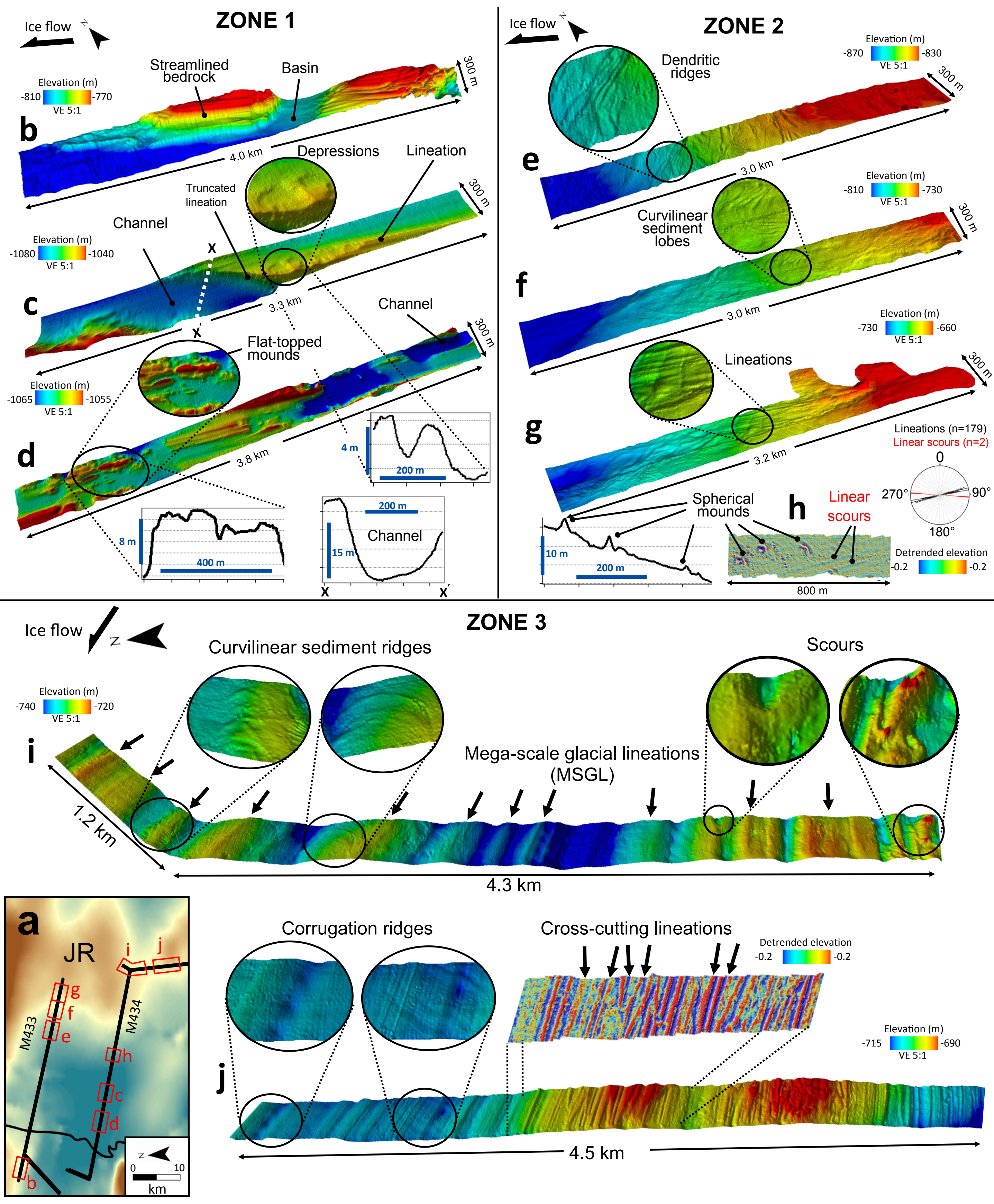

ZONE 1
Ice flow
Elevation (m)
-810
-770
VE 5:1
Streamlined bedrock
Basin
300 m
b
4.0 km
Depressions
Lineation
Truncated lineation
Channel
Elevation (m)
-1080
-1040
VE 5:1
x
c
x′
3.3 km
Channel
Flat-topped mounds
Elevation (m)
-1065
-1055
VE 5:1
d
3.8 km
4 m
200 m
8 m
400 m
200 m
Channel
15 m
x
x′
ZONE 2
Ice flow
Dendritic ridges
Elevation (m)
-870
-830
VE 5:1
e
3.0 km
Curvilinear sediment lobes
Elevation (m)
-810
-730
VE 5:1
f
3.0 km
Elevation (m)
-730
-660
VE 5:1
Lineations
g
3.2 km
Lineations (n=179)
Linear scours (n=2)
0
270°
90°
180°
Spherical mounds
h
Linear scours
10 m
200 m
800 m
Detrended elevation
-0.2
-0.2
ZONE 3
Ice flow
Curvilinear sediment ridges
Scours
Elevation (m)
-740
-720
VE 5:1
i
Mega-scale glacial lineations (MSGL)
1.2 km
4.3 km
a
JR
M433
M434
g
f
e
h
c
d
b
i
j
0
10
km
Corrugation ridges
Cross-cutting lineations
Detrended elevation
-0.2
-0.2
Elevation (m)
-715
-690
VE 5:1
j
4.5 km

Figure 4.

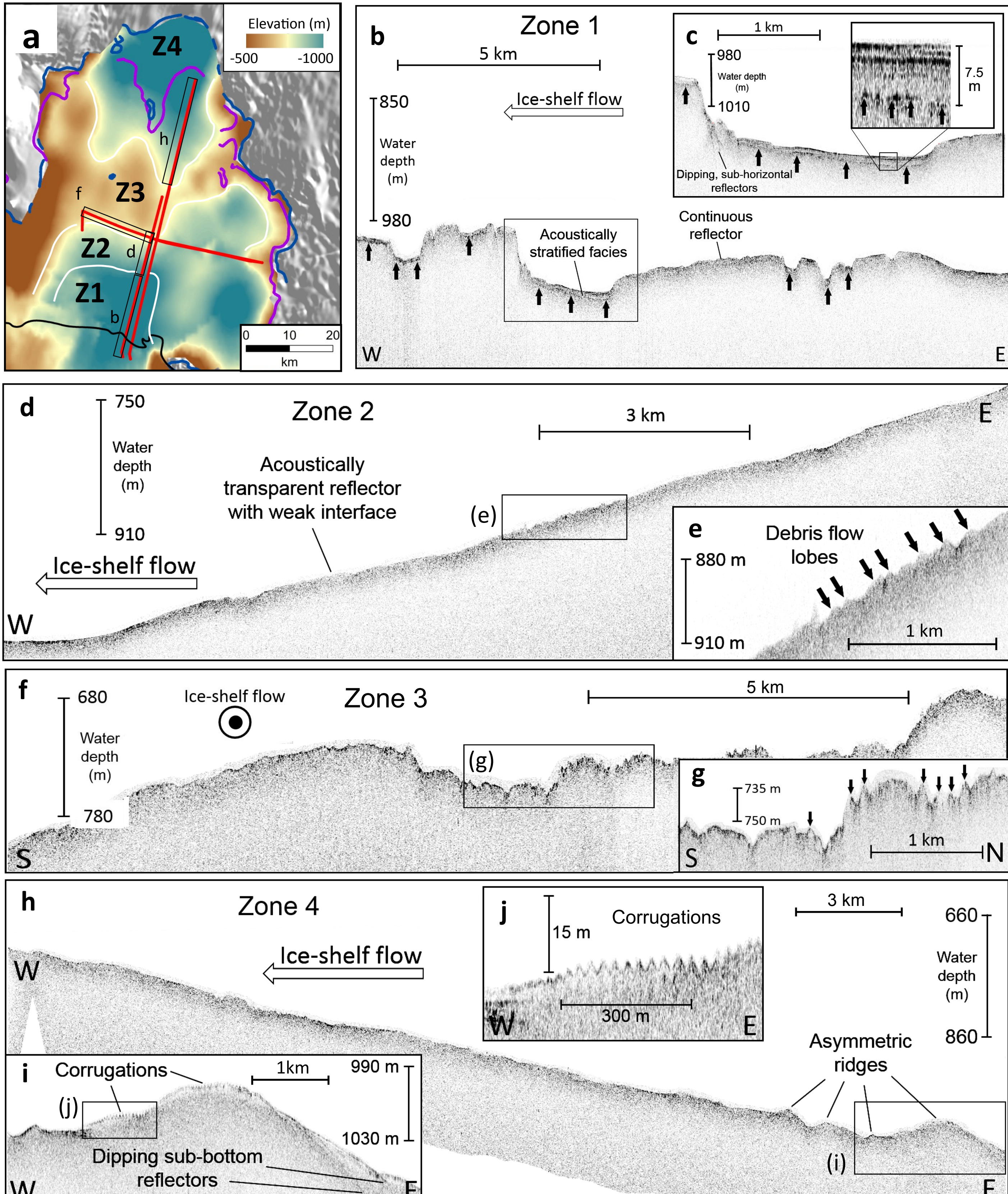

a
Elevation (m)
-500
-1000
Z4
Z3
Z2
Z1
h
f
d
b
0
10
20
km
b
Zone 1
5 km
Ice-shelf flow
850
Water depth (m)
980
c
1 km
980
Water depth (m)
1010
7.5 m
Dipping, sub-horizontal reflectors
Acoustically stratified facies
Continuous reflector
W
E
d
750
Water depth (m)
910
Zone 2
3 km
Acoustically transparent reflector with weak interface
(e)
Ice-shelf flow
e
Debris flow lobes
880 m
910 m
1 km
W
E
f
680
Water depth (m)
780
Ice-shelf flow
Zone 3
5 km
(g)
g
735 m
750 m
1 km
S
N
h
Zone 4
Ice-shelf flow
W
j
15 m
Corrugations
300 m
W
E
3 km
660
Water depth (m)
860
i
Corrugations
1km
990 m
(j)
1030 m
Dipping sub-bottom reflectors
W
E
Asymmetric ridges
(i)
E

Figure 5.

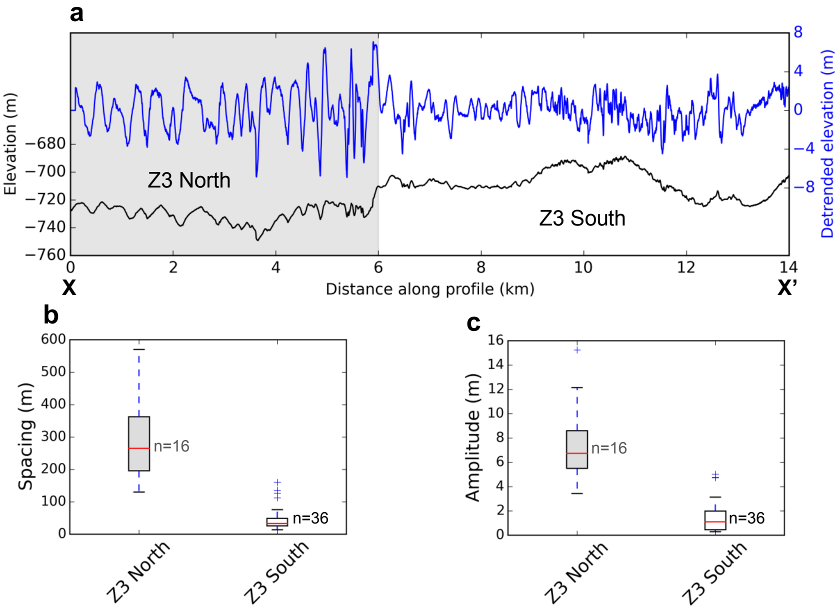
a
Z3 North
Z3 South
Elevation (m)
−680
−700
−720
−740
−760
8
4
0
−4
−8
Detrended elevation (m)
0
2
4
6
8
10
12
14
X
X'
Distance along profile (km)
b
Spacing (m)
600
500
400
300
200
100
0
n=16
n=36
Z3 North
Z3 South
c
Amplitude (m)
16
14
12
10
8
6
4
2
0
n=16
n=36
Z3 North
Z3 South

Figure 6.

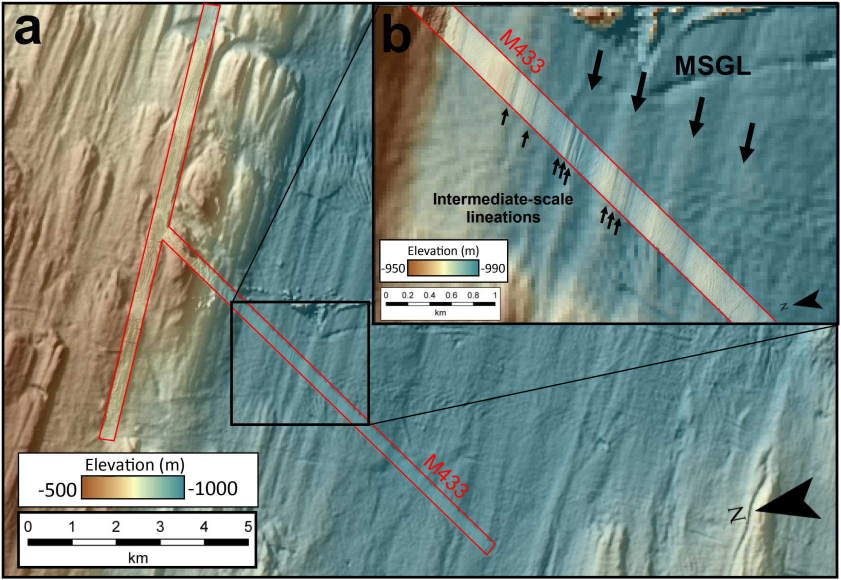
a
b
M433
MSGL
Intermediate-scale
lineations
Elevation (m)
-950
-990
0 0.2 0.4 0.6 0.8 1
km
N
M433
Elevation (m)
-500
-1000
0 1 2 3 4 5
km
N